

FORM FACTORS OF THE NUCLEON
IN THE SU (3) CHIRAL QUARK-SOLITON MODEL

Hyun-Chul Kim

Institut für Theoretische Physik II

Ruhr-Universität Bochum

D-44780 Bochum Germany

(August, 1996)

Abstract

The recent investigation on various form factors of the nucleon is reviewed in the framework of the SU (3) chiral quark-soliton model. The results for the electromagnetic and scalar form factors are in remarkable agreement with experimental and empirical data. The strange vector form factors are also discussed with the effect of the kaon cloud being considered. In addition to the form factors, the recent calculation of the tensor charges is presented.

Pacs number(s): 11.15Pg, 12.40.-y, 13.40.Gp, 14.20.Dh

Keywords: Electromagnetic form factors, scalar form factors, strange vector form factors, tensor charges, chiral quark-soliton model

Typeset using REVTeX

Invited talk given at Workshop on Electron-Nucleus Scattering, Elnba International Physics Center, 1-5 July 1996

I. INTRODUCTION

Though Quantum Chromodynamics (QCD) is believed to be the underlying theory of the strong interactions, low energy phenomena such as static properties of hadrons defy solutions based on QCD because of formidable mathematical complexities. The pertinacity of QCD in the low energy regime have led to a great deal of efforts to construct an effective theory for the strong interactions. In pursuit of this aim, the chiral quark-soliton model (QSM), also known as the semibosonized Nambu-Jona-Lasinio model, emerged as a simple and successful effective theory to describe the low energy phenomena without loss of important properties of QCD such as chiral symmetry and its spontaneous breaking.

Originally, the idea of finding the soliton in a model with quarks coupled to pions was realized by Kahana, Ripka and Soni [1] and Birse and Banerjee [2]. The bound states of the valence quarks were well explored in the model while it suffered from the vacuum instability.

Having studied the QCD instanton vacuum in the low-momentum limit, Diakonov and Petrov obtained an effective Lagrangian resembled the Nambu-Jona-Lasinio type model [4] with $2N_f$ -quark vertices. They showed that the resulting bosonized low-momentum theory is equivalent to the QSM free from the vacuum instability. In fact, the effective model by Diakonov and Petrov has several important virtues: The mechanism of the spontaneous breaking of chiral symmetry is well explained in a natural way. It provides also a renormalization scale by the inverse of the average size of the instanton $l = 600 \text{ MeV}$. In addition, the QSM throws a bridge between the nonrelativistic constituent quark model and the Skyrme model.

The baryon in this model is regarded as N_c valence quarks coupled to the polarized Dirac sea bound by a nontrivial chiral field configuration in the Hartree approximation [5,8]. The identification of the soliton as the baryon is acquired by the semiclassical collective quantization [5,9] which is performed by integrating over zero-mode fluctuations of the pion field around the saddle point. The model enables us to describe quantitatively a great deal of static properties of the nucleon such as baryon octet-decuplet mass splittings [10], magnetic

moments [11], axial constants [12,13], electromagnetic form factors [14,15] and so on (see for example a recent review [16]).

II. GENERAL FORMALISM

Let me first sketch the QSM. Because one can find the detailed formalism elsewhere, I want to present the general idea of the model briefly.

The QSM in SU(3) is characterized by a low-energy partition function in Euclidean space given by the functional integral over pseudoscalar meson and quark fields:

$$Z = \int \mathcal{D}D \mathcal{D}\psi \mathcal{D}\bar{\psi} \exp \int d^4x \bar{\psi} iD \psi ; \quad (1)$$

where iD stands for the Dirac differential operator

$$iD = (i\not{\partial} + \hat{m} + M U^5) \quad (2)$$

with the pseudoscalar chiral field

$$U^5 = \exp i^a \lambda^a_5 : \quad (3)$$

The \hat{m} denotes the matrix element of the current quark mass given by

$$\hat{m} = \text{diag}(m_u; m_d; m_s) = m_0 1 + m_3 \lambda_3 + m_8 \lambda_8 : \quad (4)$$

λ^a represents the usual Gell-Mann matrices normalized as $\text{tr}(\lambda^a \lambda^b) = 2 \delta^{ab}$. M designates the dynamical quark mass arising from the spontaneous breaking of chiral symmetry, which is in general momentum-dependent [3]. For convenience, we shall regard M as a constant and introduce the ultraviolet cutoff via the proper time regularization. The m_0, m_3 and m_8 are respectively defined by

$$m_0 = \frac{m_u + m_d + m_s}{3}; \quad m_3 = \frac{m_u - m_d}{2}; \quad m_8 = \frac{m_u + m_d - 2m_s}{2\sqrt{3}} \quad (5)$$

We assume isospin symmetry, i.e. m_3 is taken to be zero. The operator iD is expressed in Euclidean space in terms of the Euclidean time derivative ∂_4 and the Dirac one-particle Hamiltonian $H(U^5)$

$$iD = \not{\partial} + H(U^5) + m \quad (6)$$

with

$$H(U^5) = i \not{r} + M U^5 + m \quad (7)$$

and \not{r} are the well-known Dirac Hermitian matrices. The m is defined by $(m_u + m_d)=2 = m_u = m_d$, which is introduced to avoid certain divergences in some observables such as the isovector electric charge radius in the chiral limit ($m \rightarrow 0$).

Note that the effective chiral action given by Eq.(1) contains the Wess-Zumino and four-derivative Gasser-Leutwyler terms with correct coefficients in the gradient expansion. Therefore, at least the first four terms in the gradient expansion of Eq.(1) are correctly reproduced and chiral symmetry arguments do not leave much room for further modifications.

In order to calculate an observable in the QSM, we consider a correlation function:

$$\langle 0 | j_N(\mathbf{x}; \frac{T}{2}) \hat{O} J_N^Y(\mathbf{y}; \frac{T}{2}) | 0 \rangle \quad (8)$$

at large Euclidean time T . \hat{O} stands for the corresponding spin operator, while J_N^Y is the corresponding flavor operator. The J_N^Y (J_N^Y) denotes the nucleon current consisting of N_c quark fields. The corresponding matrix element can be represented by the Euclidean functional integral:

$$\begin{aligned} \langle N; p^0 \hat{O} | N; p \rangle = & \frac{1}{Z} \lim_{T \rightarrow \infty} \exp(i p_4 \frac{T}{2} - i p_4^0 \frac{T}{2}) \int_{Z'} \int_{Z''} \int_{Z'''} \\ & d^3x d^3y \exp(i p^0 y + i p x) D U^5 D D^Y \\ & J_N^Y(\mathbf{y}; T=2) \hat{O} J_N^Y(\mathbf{x}; T=2) \\ & \exp \int d^4z \bar{\psi} i D \psi \quad (9) \end{aligned}$$

With the quark fields being integrated out, Eq.(9) can be divided into two separate contributions:

$$\langle N; p^0 \hat{O} | N; p \rangle = \langle N; p^0 \hat{O} | N; p \rangle_{val} + \langle N; p^0 \hat{O} | N; p \rangle_{sea} \quad (10)$$

Schematically, the valence and sea contributions are shown in Fig.1.

The integral over chiral bosonic fields U^5 can be carried out by the saddle point method in the large N_c limit with the following Ansatz:

$$U = \begin{pmatrix} 0 & 1 \\ \frac{B}{C} U_0 & \frac{0}{A} \\ \frac{C}{A} & 0 \end{pmatrix}; \quad (11)$$

where U_0 is the $SU(2)$ chiral background field

$$U_0 = \exp[i\pi \sim P(r)]; \quad (12)$$

$P(r)$ denotes the profile function satisfying the boundary condition $P(0) = \pi$ and $P(1) = 0$.

Since the angular velocity ω_E ($1=N_c$) and the strange quark mass m_s are regarded as small parameters in our model, we expand the propagator $(iD)^{-1}$ with respect to the ω_E and m_s up to the first order:

$$\frac{1}{iD} = \frac{1}{\partial + H} + \frac{1}{\partial + H} (i\omega_E) \frac{1}{\partial + H} + \frac{1}{\partial + H} (A^y \hat{m} A) \frac{1}{\partial + H}; \quad (13)$$

Figure 2 shows the rotational $1=N_c$ corrections and m_s ones diagrammatically. The rotational $1=N_c$ corrections are of particular importance in the present model. The time-ordering of collective operators has to be taken into account in the quantization, since they do not commute in principle. The rotational $1=N_c$ corrections made it possible to solve the long-standing problem of underestimation of axial charges and magnetic moments in the QSM [12,13]. In addition, there have been arguments that the rotational $1=N_c$ corrections violate charge conjugation [17]. However, Christov et al. [18] and Wakamatsu [19] proved that the rotational $1=N_c$ corrections possess correct properties under charge conjugation. Moreover, it was shown by Praszalowicz et al. [20] that with the rotational $1=N_c$ corrections considered the QSM reproduces the result of the axial charge in the nonrelativistic quark model, i.e. $5=3$, while it gives 1 without them.

The collective $SU(3)$ Hamiltonian is no longer $SU(3)$ symmetric when the m_s corrections are taken into account. Hence, the eigenstates of the Hamiltonian are neither in a pure octet nor in a pure decuplet but in mixed state with higher representations. Dealing with the m_s as a perturbation, we can obtain the mixed $SU(3)$ baryon states:

$$\beta_{B i} = \beta_{B i} + c_{10}^B j_{10;B i} + c_{27}^B j_{27;B i} \quad (14)$$

The coefficients c_{10}^B and c_{27}^B can be found elsewhere (see for example the recent review [16]).

III. RESULTS AND DISCUSSION

I want to remark the parameters of the model for the numerical calculation, before I start to discuss the results. The present $SU(3)$ QSM contains four free parameters. Two of them are fixed in the meson sector by adjusting them to the pion mass, $m_\pi = 139$ MeV, the pion decay constant, $f_\pi = 93$ MeV, and the kaon mass, $m_K = 496$ MeV. As for the fourth parameter, i.e. the constituent mass M of up and down quarks, values around $M = 420$ MeV have been used because they have turned out to be the most appropriate one for the description of nucleon mass splittings and other observables of baryons (see ref. [16]). Hence, we fix the parameter M to 420 MeV. For the description of the baryon sector, the method of Ref. [10] is chosen, modified for a finite meson mass. The resulting strange current quark mass comes out around $m_s = 180$ MeV. With this set of fixed parameters, all the results which will be presented from now on have been calculated.

A. Electromagnetic Form Factors

Setting $\hat{O} = \hat{O}^p$ and $\hat{O} = (\hat{O}_3 + \hat{O}_8 = \hat{O}^p = 3) = 2$, we can calculate the electromagnetic form factors [15]. Figure 3 shows the electric form factors of the nucleon. In the case of the proton, the result agrees well with the empirical data [21]. As for the neutron, the result seems to be smaller than the empirical data by Paltchikov [22]. However, compared to the recent experiment conducted in Mainz [23], the $SU(3)$ result is in good agreement with it. The electric charge radii of the proton and the neutron are $\langle r_p^2 \rangle = 0.78 \text{ fm}^2$ and $\langle r_n^2 \rangle = 0.09 \text{ fm}^2$, respectively. The corresponding experimental data are $\langle r_p^2 \rangle = 0.74 \text{ fm}^2$ and $\langle r_n^2 \rangle = 0.11 \pm 0.003 \text{ fm}^2$ [24].

In dotted curves in Fig. 1, the prediction of the $SU(2)$ model is shown. As for the electric

form factor of the proton, it is comparable to the SU (2), whereas a great discrepancy is observed in the case of that of the neutron. It is partly because of the absence of m_s and terms appearing only in SU (3) and partly because of the different expectation values of the collective operators.

Figure 4 displays the magnetic form factors of the nucleon. As we can see, the momentum dependence of the magnetic form factors are well reproduced, compared to the empirical data. The m_s corrections enhance the magnetic form factors about 10% in the case of the neutron, which is not negligible to improve the prediction. The magnetic moments of the proton and the neutron are, respectively, $\mu_p = 2.39 \mu_N$ and $\mu_n = 1.76 \mu_N$, while experimental data are $\mu_p = 2.79 \mu_N$ and $\mu_n = 1.91 \mu_N$. The magnetic charge radii of the proton and the neutron are obtained as follows: $hr^2_{i_p} = 0.70 \text{ fm}^2$ and $hr^2_{i_n} = 0.78 \text{ fm}^2$. The corresponding experimental data are $hr^2_{i_p} = 0.74 \text{ fm}^2$ and $hr^2_{i_n} = 0.77 \text{ fm}^2$. On the whole, they are in remarkable agreement with the experimental data within around 15%.

In fact, one can show that any model with hedgehog symmetry cannot reproduce the experimental data of baryonic magnetic moments better than the error of 15% [11]. In that sense, the QSM lies in the upper limit of accuracy which can be attained in any hedgehog model in the case of the magnetic properties.

B. Scalar Form Factors

It is of great interest to study the scalar form factor of the nucleon [26], since it provides also a clue of strangeness in the nucleon. The analysis of the N term the momentum dependence of the scalar form factor was carried out by Gasser, Leutwyler and Sainio [27]. The results of Ref. [27] are summarized as $\sigma = 45 \pm 8 \text{ MeV}$ and $\sigma' = 60 \text{ MeV}$, and $y = 2h_N \langle \bar{s}s \rangle_N = h_N \langle \bar{u}u + \bar{d}d \rangle_N \approx 0.2$ which means a share of $h_N \langle \bar{s}s \rangle_N$ in the N term. The results indicate that the strangeness content of the nucleon in the scalar channel is not negligible, while a couple of recent theoretical works insist that there is no need to introduce a portion of strange quarks to explain the σ term [28,29]. However, though it might be

small, it is still important to consider the contribution of the strange quarks to the term in accordance with the recent experimental indication that strange quarks might play an important role of explaining the properties of the nucleon.

Figure 5 draws the scalar form factor of the nucleon. The error bar presented in Fig. 5 stands for the empirical analysis due to Gasser, Leutwyler and Sainio. As shown in Fig. 5 our theoretical prediction is in good agreement with Ref. [27]. The m_s corrections seem to be negligible in the scalar form factor. However, they play an important role of suppressing the strangeness contribution: The value of y with the m_s corrections is 0.27 while $y = 0.48$ without the m_s corrections. It implies that though the m_s corrections have a tiny effect on the magnitude of the scalar form factor, it leads to a large suppression of the y . The difference

$\langle \bar{u}u \rangle (2m^2) (0)$ we have obtained is 18.18 MeV. This value is very close to what Ref. [27] extracted, i.e. $\langle \bar{u}u \rangle (2m^2) (0) = 15.2 \pm 0.4$ MeV. The prediction of the QSM for the scalar radius $\langle r^2 \rangle_N^S$ is 1.5 fm^2 which is also comparable to the empirical value obtained by Ref. [27] $\langle r^2 \rangle_N^S \approx 1.6 \text{ fm}^2$.

C. Strange Vector Form Factors

The strangeness content of the nucleon in the vector channel is one of hot issues these days. While a great deal of theoretical works pile up, there is no clear theoretical consensus and no evident experimental judgment yet.

Encouraged by successful results of the scalar, electromagnetic and axial properties in the SU(3) QSM, it is of great interest to investigate the strange vector form factors in the same framework [30]. However, before we pursue the study of the strange vector form factors, we need to take into account the kaonic effect properly in line with the recent theoretical calculations incorporating the kaonic loops [31]. From this theoretical point of view, the strangeness in the nucleon can be interpreted in terms of the K or \bar{K} components. Figure 6 displays a schematic diagram of explaining how the strangeness arises in the nucleon. The diagram shown in the left-hand side of Fig. 6 can be redrawn in terms of quarks. In fact,

the nucleon is known to consist of three valence quarks, i.e. uud. When one of the u quarks is hit by the external strange vector current as shown in Fig. 6, the ss pair is created and rearranged so that we may have quark compositions uds and us. They correspond respectively to Λ and K^+ . This explains that we have the contribution from the valence part as well as the sea part to the strange vector form factors, though the nucleon itself does not include any strange valence quark.

As is explained above, kaons play a dominant role in describing the strange vector form factors. The QSM discussed up to now does not include the kaon cloud which is believed to be of little importance in the former calculation except for the neutron electric form factor [32]. However, to treat the strange vector form factors, we have to take the effect of the kaon cloud into account properly. To do so, we have incorporated the kaonic tails selfconsistently in the profile $P(r)$ in Eq.(12) at the expense of the pion tails.

Figure 7 shows the strange vector form factors. The effect of the kaon cloud is in particular prominent in the case of the strange electric form factor. As shown in Fig. 7, the replacement of the pion cloud by the kaon one brings about a sizable decrease of the strange electric form factor almost by a factor of three. This remarkable result is in line with the recent investigation of the kaonic effects on the neutron electric form factor [32]. Such a drastic reduction of the strange electric form factor can be easily understood explicitly by evaluating the strange electric radii. In any hedgehog model the strange radii depend on the inverse of the meson mass which suppresses the tail of the profile, i.e. $hr^2 i_s = 1/m$. From such a behavior of the $hr^2 i_s$, we can derive the relation

$$\frac{hr^2 i_s^{\text{Sachs}} = m}{hr^2 i_s^{\text{Sachs}} = m_K} = \frac{m_K}{m}, \quad (15)$$

Eq.(15) explains the decrease of the $hr^2 i_s$ with $m = m_K$.

Though the strange magnetic form factor is not changed as much as the strange electric one, the effect of the kaon cloud is still noticeable. In contrast to the strange electric form factor, the kaon cloud enhances the magnitude of the strange magnetic one almost 50%. As a result, by replacing the pion cloud by the kaon one, the strange magnetic moment μ_s is

brought from 0.44_N to 0.68_N .

In addition, I want to mention a preliminary experimental result of the strange magnetic moment announced by McKewen [33] in this workshop. Surprisingly, his finding is positive. It implies that it conflicts with almost all of the theoretical models including the present model. If the experimental result turns out to be correct, the present simple picture will not be enough to describe the strange vector form factors. A more sophisticated and higher order corrections should be considered. However, we still anticipate more compiled experimental data to enlighten us on it.

D. Tensor Charges

Finally, I want shortly to present a recent calculation of the tensor charges of the nucleon [34]. The tensor charge q_T is related to the transverse quark distribution $h_1(x)$. However, $h_1(x)$ is not measurable in inclusive deep-inelastic scattering. That is the reason why it has not been extensively studied for long. In fact, Ralston and Soper [35] proposed the $h_1(x)$ which can be measured in polarized Drell-Yan processes almost 20 years ago. Recently, it was also suggested that the $h_1(x)$ can be measured in other exclusive hard reactions [36-38].

Jaffe and Ji demonstrated that the first moment of the $h_1(x)$ is related to the tensor charge of the nucleon:

$$\int_0^1 dx h_1(x) = q_T \quad (16)$$

where $h_1(x)$ is an antiquark transversity distribution. Setting $\hat{O} = \hat{O}^a$ in Eq.(8), we can evaluate the tensor charges q_T^a in the \overline{MS} , which are linearly related to q_T . Note that the tensor charges depend on the renormalization scale, though their dependence on it is very weak. The normalization point pertinent to the \overline{MS} is not determined from the first principle. However, as mentioned in section I, the renormalization point in the \overline{MS} has been chosen by $\mu = 600 \text{ MeV}$, but there may be a factor of order unity.

In Tables I-II the results of the tensor charges are summarized. As shown in Table I the rotational $1=N_c$ corrections are of great significance numerically, while the m_s corrections are

relatively small. In contrast to the axial charges, the tensor ones in the QSM are closer to their values in the nonrelativistic constituent quark model and in particular the strangeness contribution to the tensor charge s is compatible with zero, while that to the axial ones s in the QSM is negative and distinctive from zero [39]. This difference between the tensor charges and the axial ones can be explained by calculating them in the gradient expansion and scrutinizing their dependence on the size of the soliton [40].

IV . S U M M A R Y

My aim in this talk has been to review the recent investigation on various form factors of the nucleon in the SU(3) chiral quark-soliton model (QSM). The rotational $1=N_c$ and linear m_s corrections were taken into account. The only parameter we have in the model is the constituent quark mass M which is fixed to 420 MeV by the mass splitting of the SU(3) baryon octet and decuplet. The results for the electromagnetic and scalar form factors are in remarkable agreement with experimental and empirical data within about 15%.

The strange vector form factors were also discussed. The effect of kaon cloud turns out to be very large. By taking into account this kaonic effect, the strange charge radius is reduced to be almost 3 times smaller than that without the kaon cloud, while the magnitude of the strange magnetic moment is increased.

The tensor charges of the nucleon are presented in the same framework. The QSM predicts the number of the transversely polarized strange quarks s in the transversely polarized nucleon compatible with zero, whereas it yields the negative nonzero number of the polarized strange quarks s in the longitudinally polarized nucleon, which is consistent with the corresponding experimental value.

A C K N O W L E D G M E N T S

The works presented in this talk were done in collaboration with A. B. Metz, M. V. Polyakov, C. Schneider, T. Watabe and K. Goeke. The work is supported by the BMBF, the DFG,

and the COSY project (Jülich). I am grateful to O. Benhar and A. Fabrocini for the warm hospitality in E. Iba.

TABLES

TABLE I. Tensor charges $g_T^{(0)}$, $g_T^{(3)}$ and $g_T^{(8)}$ with the constituent quark mass $M = 420$ MeV. The current quark mass m_s is chosen as $m_s = 180$ MeV. The natural model predictions are given by $O(1; m_s^1)$.

	$O(0; m_s^0)$	$O(1; m_s^0)$	$O(1; m_s^1)$
$g_T^{(0)}$	0	0.69	0.70
$g_T^{(3)}$	0.79	1.48	1.54
$g_T^{(8)}$	0.09	0.48	0.42

TABLE II. Each flavor contribution to the tensor charges as varying the constituent quark mass M . The current quark mass m_s is chosen as $m_s = 180$ MeV.

M [MeV]	u	d	s
420	1.12	-0.42	-0.008

REFERENCES

- [1] S. Kahana, G. Ripka and V. Soni, Nucl. Phys. A 415 (1984) 351.
- [2] M. S. Birse and M. K. Banerjee, Phys. Lett. 136B (1984).
- [3] D. D. Iakonov and V. Petrov, Nucl. Phys. B 272 (1986) 457.
- [4] Y. Nambu and G. Jona-Lasinio, Phys. Rev. 122 (1961) 345; Phys. Rev. 124 (1961) 246.
- [5] D. D. Iakonov, V. Petrov and P. P. Pobylytsa, Nucl. Phys. B 272 (1988) 809.
- [6] H. Reinhardt and R. Wunsch, Phys. Lett. 215B (1988) 577.
- [7] Th. Meiner, F. G. Murrer and K. Goebel, Phys. Lett. 227B (1989) 296.
- [8] M. Wakamatsu and H. Yoshiki, Nucl. Phys. A 524 (1991) 561.
- [9] G. S. Adkins, C. R. Nappi and E. Witten, Nucl. Phys. B 228 (1983) 552.
- [10] A. Blotz, D. D. Iakonov, K. Goebel, N. W. Park, V. Petrov and P. V. Pobylytsa, Phys. Lett. B 287 (1992) 29.
- [11] H.-C. Kim, M. V. Polyakov, A. Blotz and K. Goebel, Nucl. Phys. A 598 (1996) 379.
- [12] M. Wakamatsu and T. Watabe, Phys. Lett. 312B (1993) 184.
- [13] C. V. Christov, A. Blotz, K. Goebel, P. Pobylytsa, V. Petrov, M. Wakamatsu, and T. Watabe, Phys. Lett. 325B (1994) 467.
- [14] Ch. Christov, A. Z. Gorski, K. Goebel and P. V. Pobylytsa, Nucl. Phys. A 592 (1995) 513.
- [15] H.-C. Kim, A. Blotz, M. V. Polyakov, and K. Goebel, Phys. Rev. D 53 (1996) 4013.
- [16] C. V. Christov, A. Blotz, H.-C. Kim, P. Pobylytsa, T. Watabe, Th. Meissner, E. Ruiz Arriola and K. Goebel, Prog. Part. Nucl. Phys. 37 (1996) 91.
- [17] J. Schechter and H. Weigel, Mod. Phys. Lett. A 10 (1995) 885; Phys. Rev. D 51 (1995) 6296.

- [18] Chr.V. Christov, K. Goeke, and P.V. Pobylitsa, Phys. Rev. C 52 (1995) 425.
- [19] M. Wakamatsu, Phys. Lett. 349B (1995) 204.
- [20] M. Praszalowicz, A. Błotz and K. Goeke, Phys. Lett. 354 B (1995) 415.
- [21] G. Hohler et al, Nucl. Phys. B 114 (1976) 505.
- [22] S. Platchkov et al, Nucl. Phys. A 510 (1990) 740.
- [23] M. Meyerhofer et al, Phys. Lett. B 327 (1994) 201.
- [24] S. Kopecky, P. Riehs, J.A. Harvey and N.W. Hill, Phys. Rev. Lett. 74 (1995) 2427.
- [25] E.E.W. Bruins et al, Phys. Rev. Lett. 75 (1995) 21.
- [26] H.-C. Klein, A. Błotz, C. Schneider, and K. Goeke, Nucl. Phys. A 596 (1996) 415.
- [27] J. Gasser, H. Leutwyler, and M.E. Sainio, Phys. Lett. 253B (1991) 252; Phys. Lett. 253B (1991) 260.
- [28] S.D. Bass, Phys. Lett. 329B (1994) 358.
- [29] R.D. Ball, S. Forte, and J. Tigg, Nucl. Phys. B 428 (1994) 485.
- [30] H.-C. Klein, T. Watabe, and K. Goeke, RUB-TP II-11/95 [hep-ph/9606440] (1996).
- [31] M.J. Musolf and M. Burkardt, Z. Phys. C 61 (1994) 433.
- [32] T. Watabe, H.-C. Klein, and K. Goeke, RUB-TP II-17/95 (1995).
- [33] R.D. Muckeown, MAP-202 [hep-ph/9607340] and see also the present proceedings.
- [34] H.-C. Klein, M.V. Polyakov, and K. Goeke, Phys. Lett. B in print (1996).
- [35] J. Ralston and D. Soper, Nucl. Phys. B 152, 109 (1979).
- [36] R.L. Jaffe and X. Ji, Phys. Rev. Lett. 71, 2547 (1993).
- [37] J. Collins, Nucl. Phys. B 394 (1993) 169.

[38] C. Bouchery and J. Soer, Nucl. Phys. B 243, 329 (1994); Nucl. Phys. B 445, 341 (1995).

[39] A. Blotz, M. Praszalowicz, and K. Goeke, Phys. Rev. D 53 (1996) 485.

[40] H.-C. Klein, M. V. Polyakov, and K. Goeke, Phys. Rev. D 53 (1996) R4715.

Figure Captions

Figure 1: The valence and sea contributions to an observable. The left panel draws a schematic diagram for the valence contribution, while the right one is for the sea contribution. The solid lines denote the N_c valence quarks, whereas the loops designate the polarized Dirac sea. The wiggled line stands for the corresponding external current to the observable h_i .

Figure 2: The rotational $1=N_c$ and m_s corrections. The upper panel shows the rotational $1=N_c$ corrections, while the lower panel is for the m_s corrections. The solid lines denote the N_c valence quarks, whereas the loops designate the polarized Dirac sea. The wiggled line stands for the corresponding external current to the observable h_i .

Figure 3: The electric form factors of the proton and the neutron. The left panel displays that of the proton, while the right panel is for the neutron. The solid curve corresponds to the strange quark mass $m_s = 180 \text{ MeV}$, while the dashed curve draws that without m_s . The dotted curve shows the case of the SU(2) model. $M = 420 \text{ MeV}$ is chosen for the constituent quark mass. The empirical data for the proton are taken from Hohler et al. [21] while for the neutron they are taken from Platchkov [22].

Figure 4: The magnetic form factors of the proton and the neutron. The left panel displays that of the proton, while the right one is for the neutron. The solid curve corresponds to the strange quark mass $m_s = 180 \text{ MeV}$, while the dashed curve draws that without m_s . The dotted curve shows the case of the SU(2) model. $M = 420 \text{ MeV}$ is chosen for the constituent quark mass. The empirical data are taken from Hohler et al. [21]. The experimental data for the neutron magnetic form factor (open triangle) are due to Bruins et al. [25].

Figure 5: The scalar form factor of the nucleon (t). The solid curve displays the case of $m_s = 148.49 \text{ MeV}$, while the dashed curve shows that without m_s . The error bar denotes the empirical value from Gasser et al. [27].

Figure 6: A schematic diagram of the kaon effect on the strange vector form factors. The left panel displays the K^+ component of the strange vector form factors, while the right one shows the same component in a quark language.

Figure 7: The strange vector form factors of the nucleon. The left one displays the strange electric form factor, while the right panel draws the strange magnetic form factor. The solid curve corresponds to the $\mu = m_K$, while dashed curve draws $\mu = m$. The constituent quark mass M and m_s are 420 MeV and 180 MeV , respectively.

Figures

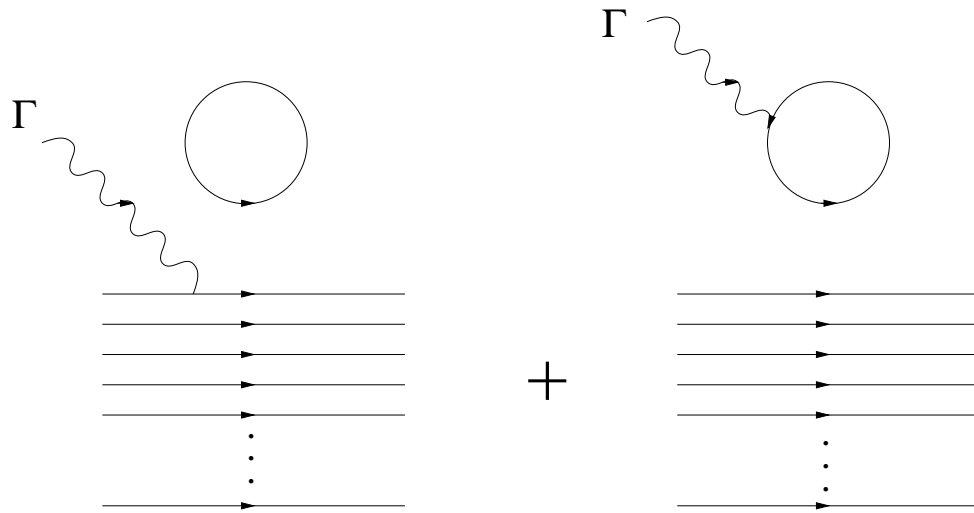


Figure 1

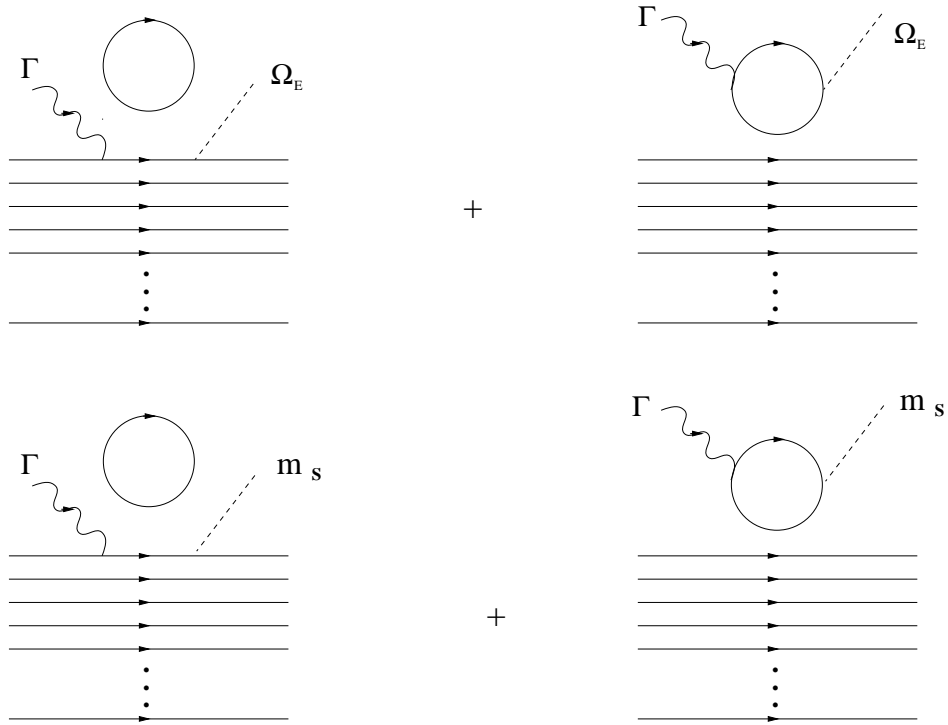


Figure 2

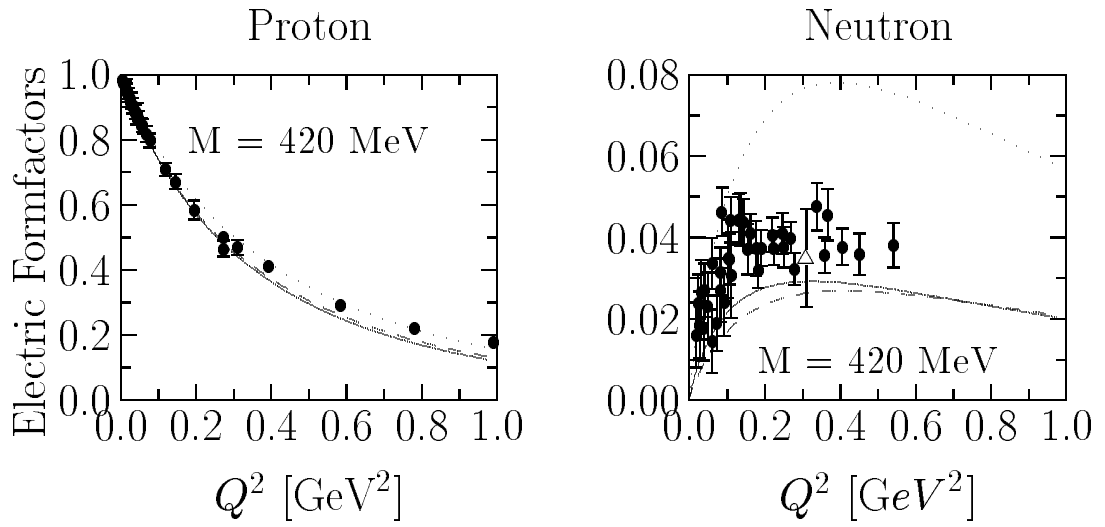


Figure 3

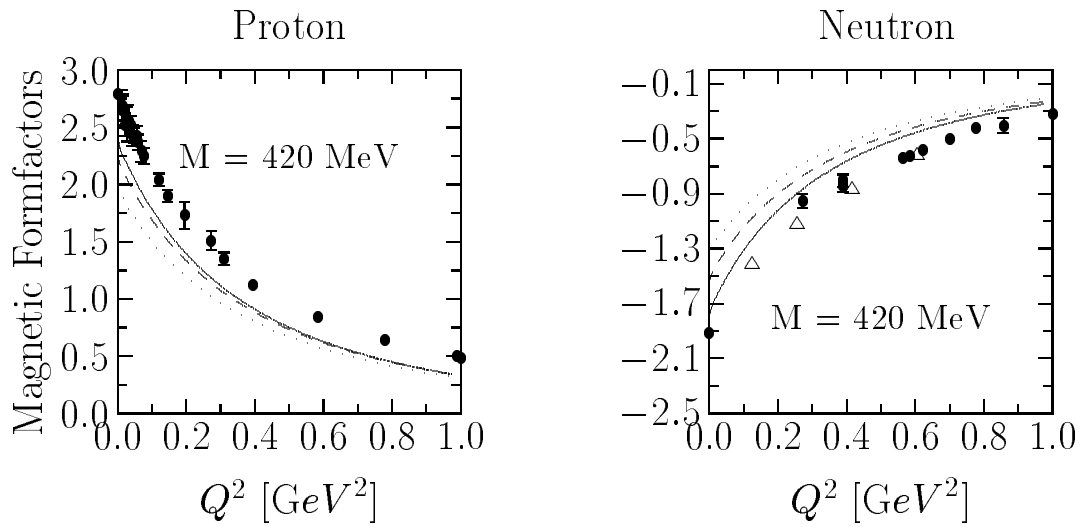


Figure 4

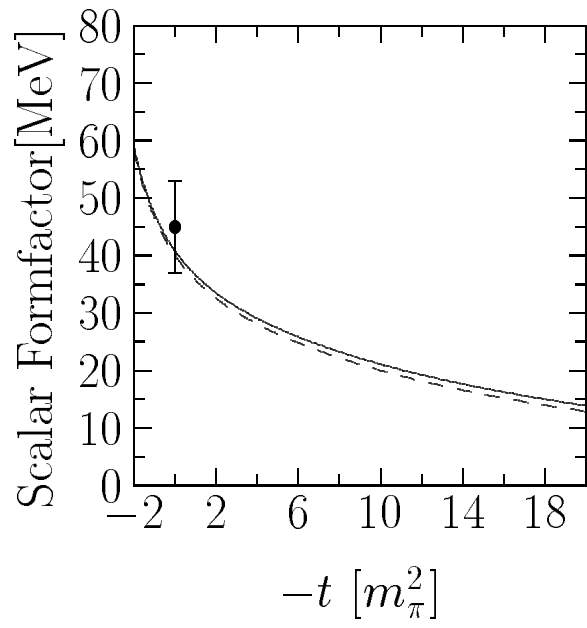


Figure 5

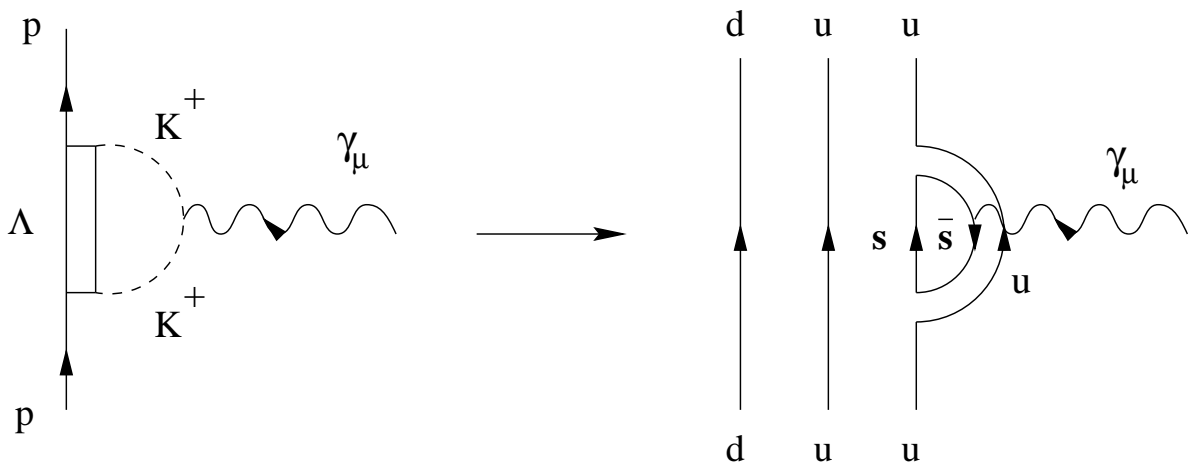


Figure 6

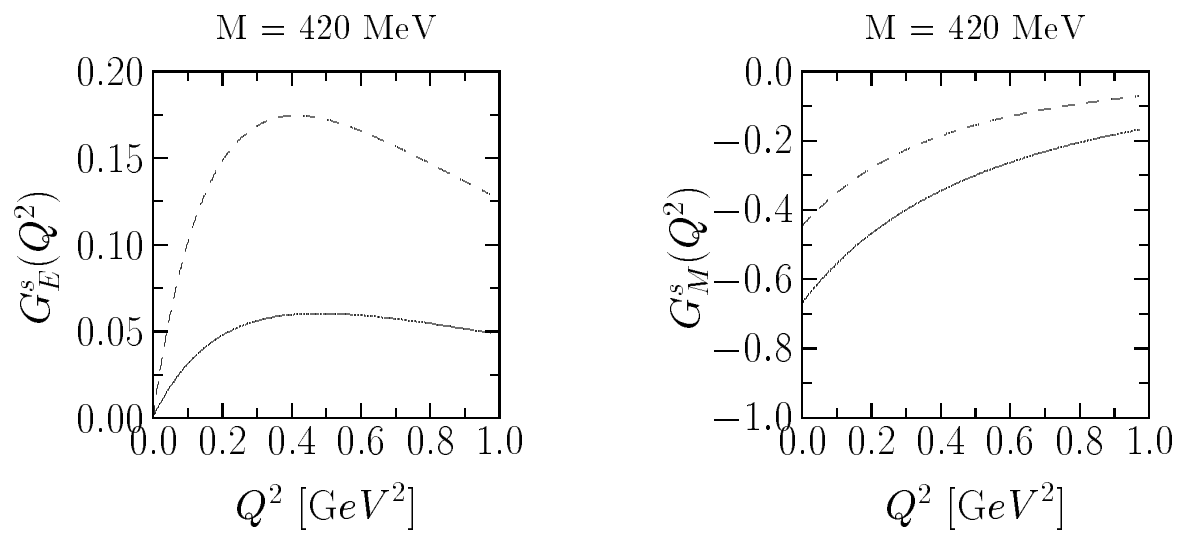


Figure 7